Supplementary Materials for

Tubulin Lattice in Cilia is in a Stressed Form Regulated by Microtubule Inner Proteins

Muneyoshi Ichikawa[1], Ahmad Abdelzaher Zaki Khalifa[1], Shintaroh Kubo[3], Daniel Dai[1], Kaustuv Basu[2], Mohammad Amin Faghfor Maghrebi[1], Javier Vargas[1], Khanh-Huy Bui[1,*]

[*] Corresponding author. E-mail: huy.bui@mcgill.ca

This PDF file includes:

Supplementary Figure Caption
Figs. S1 to S5
Tables S1 to S5
Captions for Movies S1, S2, S3, S4 and S5

www.pnas.org/cgi/doi/10.1073/pnas.1911119116

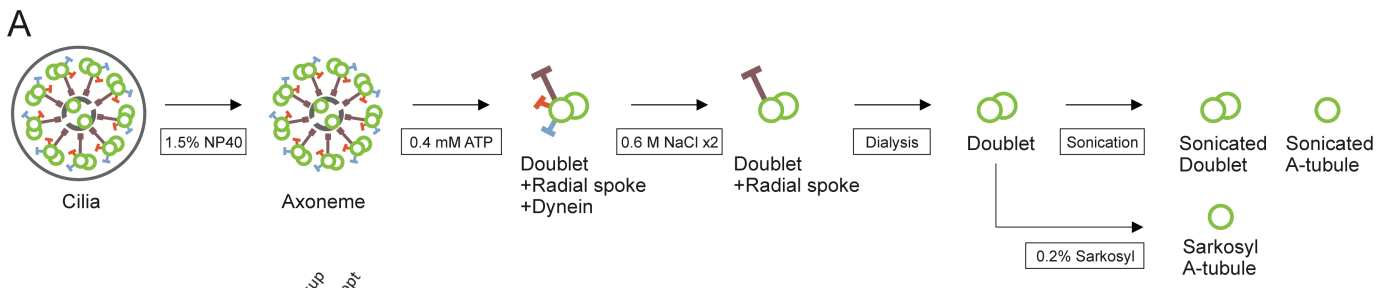
A
Cilia
1.5% NP40
Axoneme
0.4 mM ATP
Doublet
+Radial spoke
+Dynein
0.6 M NaCl x2
Doublet
+Radial spoke
Dialysis
Doublet
Sonication
Sonicated
Doublet
Sonicated
A-tubule
0.2% Sarkosyl
Sarkosyl
A-tubule

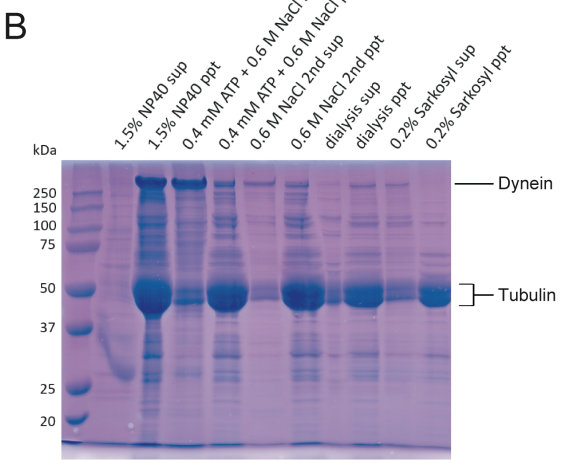
B
1.5% NP40 sup
1.5% NP40 ppt
0.4 mM ATP + 0.6 M NaCl sup
0.4 mM ATP + 0.6 M NaCl ppt
0.6 M NaCl 2nd sup
0.6 M NaCl 2nd ppt
dialysis sup
dialysis ppt
0.2% Sarkosyl sup
0.2% Sarkosyl ppt
kDa
250
150
100
75
50
37
25
20
Dynein
Tubulin

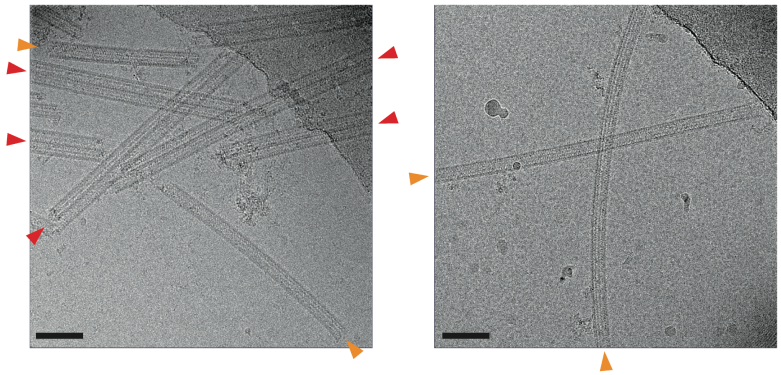
C
D

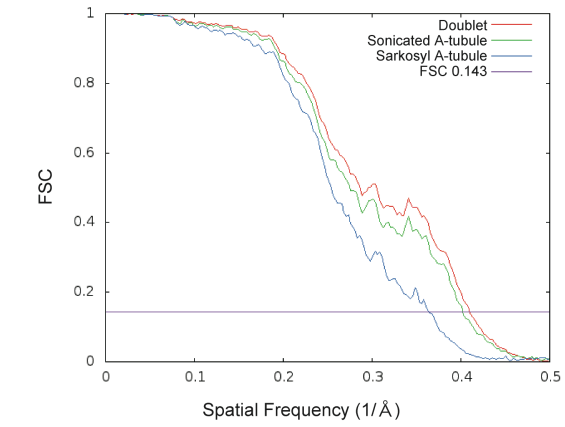
E
Doublet
Sonicated A-tubule
Sarkosyl A-tubule
FSC 0.143
FSC
Spatial Frequency (1/Å)

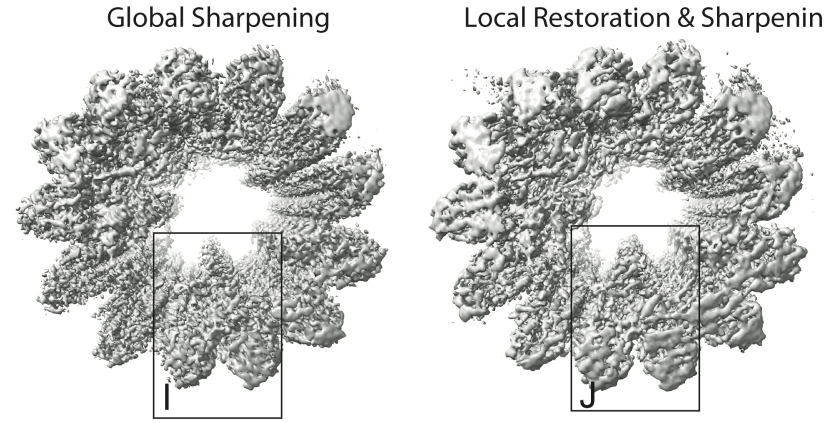
G
Global Sharpening
H
Local Restoration & Sharpening
I
J

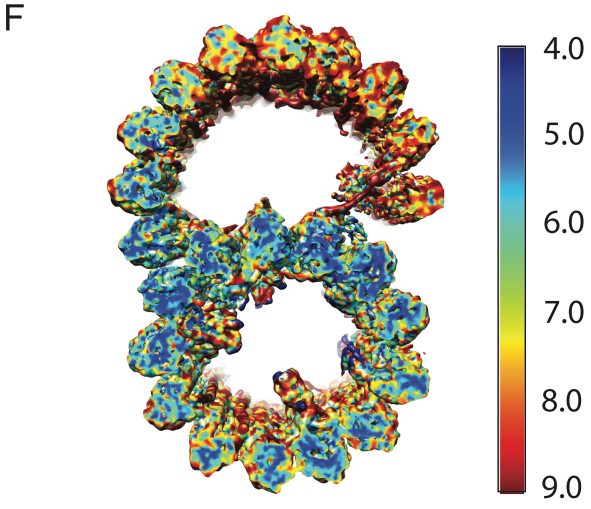
F
4.0
5.0
6.0
7.0
8.0
9.0

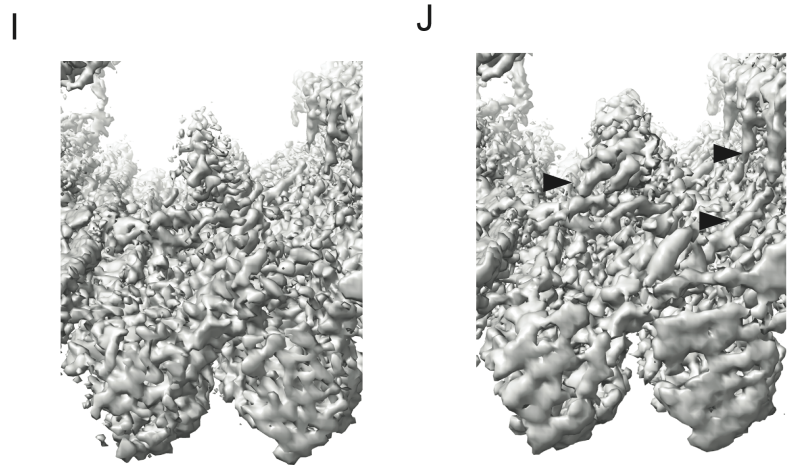
I
J

Fig. S1. Related to doublet microtubule structure.

(A) Schematics of fractionation of the axoneme in this study. Doublets were split from axoneme, and outside proteins were removed to obtain a simpler sample for cryo-EM. A-tubules were obtained by either sonication or sarkosyl treatment. (B) SDS-PAGE gel of the fractionated axoneme. From the gel, the sarkosyl-treated fraction was less complex than the doublet fraction consistent with the missing densities in the EM result. (C) A typical cryo-EM image of the doublet fraction shows both doublets (red arrowheads) and A-tubules (orange arrowheads) due to the sonication process. (D) A representative cryo-EM image of the sarkosyl-treated fraction shows the A-tubules (orange arrowheads). Scale bars in (C and D), 100 nm. (E) Gold-standard Fourier Shell Correlation of the doublet, sonicated and sarkosyl A-tubule maps. (F) Local resolution estimation of the doublet using MonoRes. The A-tubule, in general, has good resolution while the resolution of the B-tubule is lower due to the flexibility without the inner junction. (G) and (H) The sarkosyl A-tubule sharpened globally by Relion and locally by local restoration and sharpening. The magnified views of the structures are shown in (I) and (J). It is clearly shown that local restoration and sharpening improved connectivity in the structure.

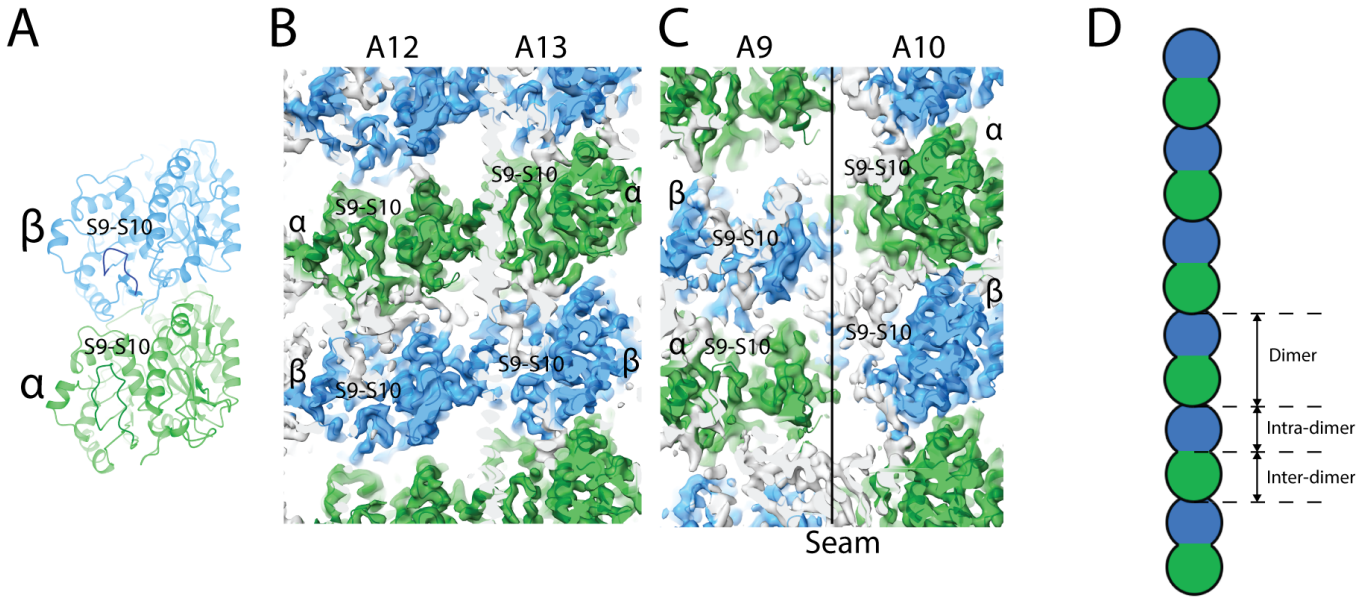
A
β
S9-S10
S9-S10
α
B
A12
A13
S9-S10
α
S9-S10
α
β
S9-S10
S9-S10
β
C
A9
A10
α
S9-S10
β
S9-S10
β
S9-S10
α
S9-S10
Seam
D
Dimer
Intra-dimer
Inter-dimer

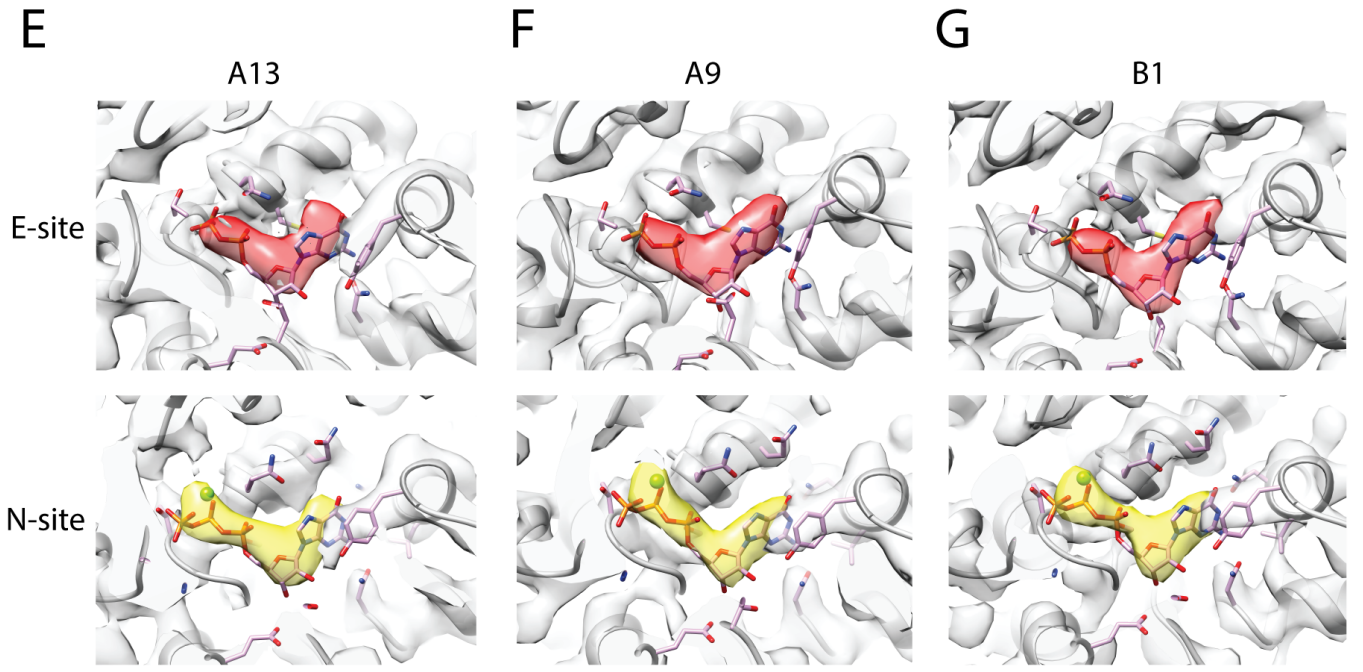
E
A13
F
A9
G
B1
E-site
N-site

Fig. S2. Determination of α- and β-tubulins and nucleotide states in the doublet

(A) A view of tubulin model shows the clear difference between the loop S9-S10 of α- and β-tubulins. S9-S10 loop of β-tubulin is much shorter than that of α-tubulin. Luminal views of α- and β-tubulins in PF A12 and A13 (B), and PF A9 and A10 (C) show clear visualization of the S9-S10 loop and also identify the seam between A9 and A10. (D) A schematic of how we measured the dimer distance. (E-G) Nucleotide densities in tubulins. Densities corresponding to GTP are observed in α-tubulins of PF A13 (E), A9 (F) and B1 (G) while densities corresponding to GDP are observed in β-tubulins of PF A13 (E), A9 (F) and B1 (G).

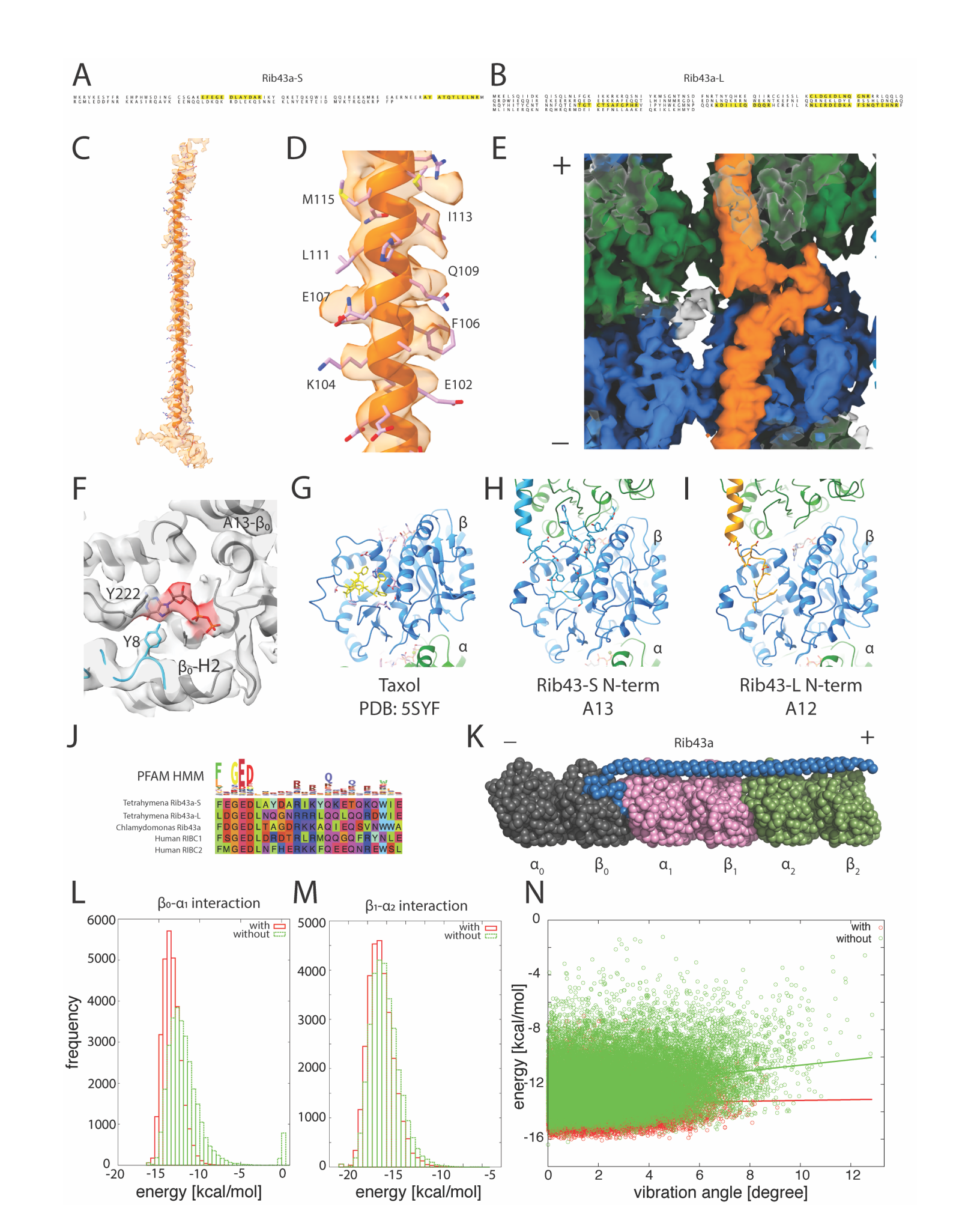
A
Rib43a-S
B
Rib43a-L
C
D
M115
I113
L111
Q109
E107
F106
K104
E102
E
+
–
F
A13-β0
Y222
Y8
β0-H2
G
β
α
Taxol
PDB: 5SYF
H
β
α
Rib43-S N-term
A13
I
β
α
Rib43-L N-term
A12
J
PFAM HMM
Tetrahymena Rib43a-S
Tetrahymena Rib43a-L
Chlamydomonas Rib43a
Human RIBC1
Human RIBC2
K
–
Rib43a
+
α0
β0
α1
β1
α2
β2
L
β0-α1 interaction
with
without
frequency
energy [kcal/mol]
M
β1-α2 interaction
with
without
energy [kcal/mol]
N
with
without
energy [kcal/mol]
vibration angle [degree]

Fig. S3: Data related to Rib43a-S and Rib43a-L

(A-B) Peptide coverage of Rib43a-S (A) and Rib43a-L (B) from the mass spectrometry of sarkosyl A-tubule. (C) Model of amino acids 60-172 of Rib43a-L inside its segmented density. (D) A close-up of the H1 region of Rib43a-L. (E) The junction region of Rib43a-L is connected using a lower threshold of 0.019. In comparison, the threshold used for the junction region of Rib43a-L in Fig. 3G is 0.04. (F) Residue Y8 from Rib43a-S could interact with GDP from β-tubulin, similar to Y222 of β-tubulin. (G-I) Models of taxol (PDB: 5SYF) (G), N-terminus of Rib43a-S (H) and N-terminus of Rib43a-L (I) bind to β-tubulin. (J) Sequence alignment and Hidden Markov Model (1) of Rib43a from *Tetrahymena*, *Chlamydomonas* and human. (K) Overview of the MD simulation setup. Model of three tubulin dimers (each chain is named as α_0, β_0, α_1, β_1, α_2 and β_2) were analyzed by MD simulation with or without Rib43a-S model. (L-M) Histogram of energy between β_0 and α_1 (L) and between β_1 and α_2 (M) obtained from 30 coarse-grained MD simulations with (red box) and without (green box) Rib43a-S. With Rib43a bound, the energy between β-tubulin of the first dimer and α-tubulin of the second dimer is lower, meaning that the structure is more stable with Rib43a-S. There is an insignificant difference in energy between β_1 and α_2, suggesting that the N-terminus has a stronger effect in stabilizing the tubulin lattice. (N) The correlation of the energy between β_0 and α_1 and the bending angle of the filament from the 30 coarse-grained MD simulations with (red dot) and without (green dot) Rib43a-S. Each of the two straight lines (red and green) is a fitted line between the energy and the angle with and without Rib43a-S by the least-square method ($y = 0.0279x - 13.5$ and $y = 0.199x - 12.6$, respectively). Without Rib43a, tubulins become less stable (higher energy) as the tubulin lattice bends (larger vibration angle). In contrast, when Rib43a is bound, tubulins stay in a rather consistent energy state even with more bending.

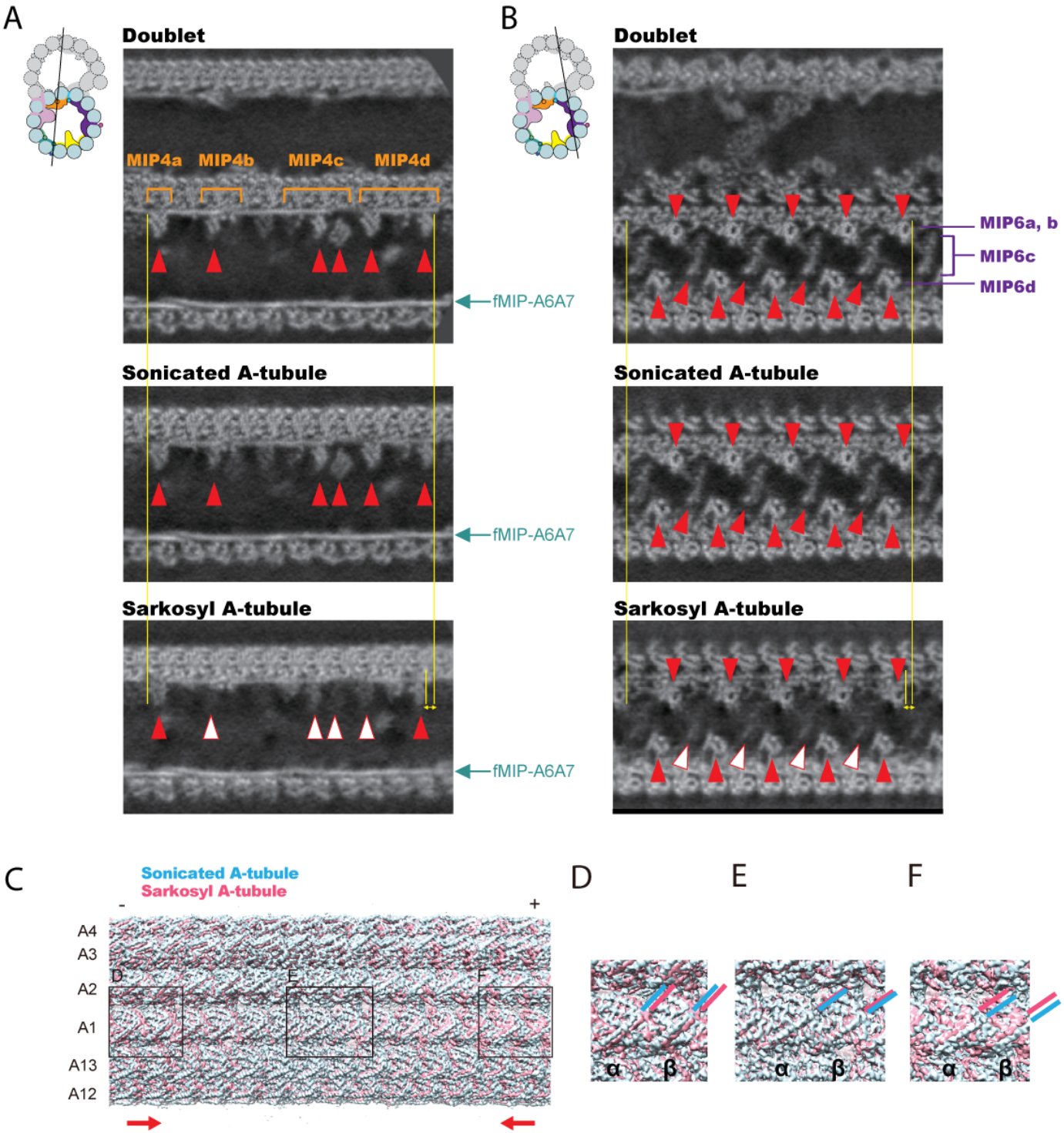
A
Doublet
MIP4a
MIP4b
MIP4c
MIP4d
fMIP-A6A7
Sonicated A-tubule
fMIP-A6A7
Sarkosyl A-tubule
fMIP-A6A7
B
Doublet
MIP6a, b
MIP6c
MIP6d
Sonicated A-tubule
Sarkosyl A-tubule
C
Sonicated A-tubule
Sarkosyl A-tubule
-
+
A4
A3
A2
A1
A13
A12
D
E
F
D
E
F
α
β
α
β
α
β

Fig. S4. Comparison of MIPs from the doublet, sonicated A-tubule and sarkosyl A-tubule maps. (A and B) Slices through the maps of the doublet, sonicated A-tubule and sarkosyl A-tubule. Black lines in the schematics indicate the locations of the slices. MIP4 and MIP6 densities are preserved in the sonicated A-tubule structure as shown by red arrowheads. Missing parts of these MIPs in the sarkosyl A-tubule map are indicated by empty arrowheads. fMIP-A6A7 densities are shown by arrows in (A). Yellow lines and double-headed arrows show the shifts of the MIPs in the longitudinal direction due to compaction of the tubulin lattice in sarkosyl A-tubule. (C-F) Comparison of the density maps of sonicated and sarkosyl A-tubules. In the middle part, tubulins fit well to the density map as in (E). On the other hand, as it gets closer to both ends, tubulin densities from sarkosyl A-tubule map appear shifted toward the middle (D and F), which means that sarkosyl A-tubule tubulin lattice is shorter than that of sonicated A-tubule. Red arrows indicate the tubulin shift directions from both + and - ends. Locations of helix H12 of tubulin are indicated by pink or blue lines.

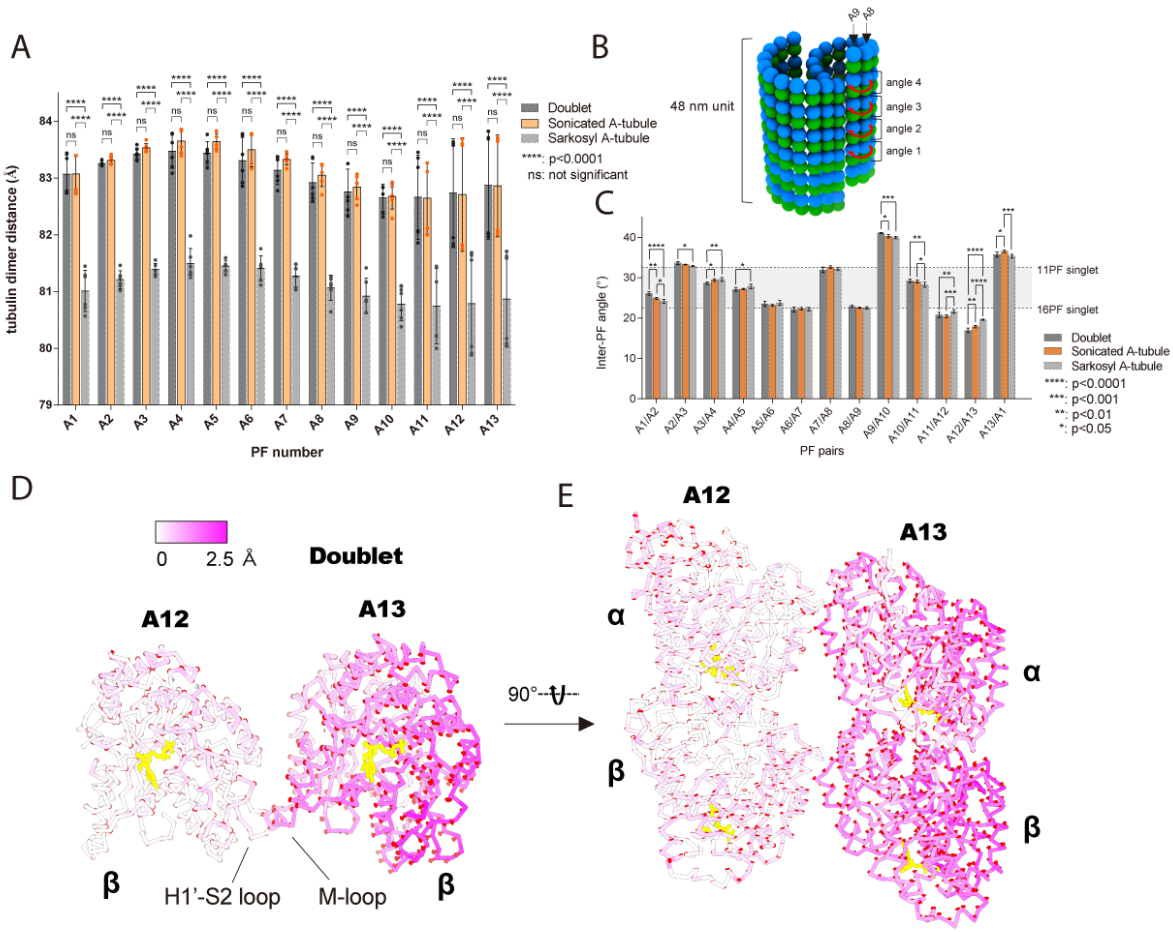
A
B
C
D
E
tubulin dimer distance (Å)
PF number
Doublet
Sonicated A-tubule
Sarkosyl A-tubule
****: p<0.0001
ns: not significant
48 nm unit
angle 4
angle 3
angle 2
angle 1
A9
A8
Inter-PF angle (°)
11PF singlet
16PF singlet
PF pairs
***: p<0.001
**: p<0.01
*: p<0.05
0
2.5 Å
Doublet
A12
A13
β
H1'-S2 loop
M-loop
90°
α

Fig. S5. Data related to longitudinal tubulin dimer distance and curvature.

(A) Plot of tubulin dimer distances from the sonicated A-tubule map. Values of the A-tubule from the doublet and sarkosyl A-tubule maps from Fig. 5A are shown in gray for comparison. For statistical analysis, two-way ANOVA followed by Tukey's multiple comparison test was performed. For all PFs, changes between the doublet and sonicated A-tubule are not significant ($p > 0.01$). The sonicated A-tubule also shows a bimodal distribution in the PF ribbon region. (B) Schematic of PF angle measurements. Angles were measured using four tubulin pairs from each PF pair in the 48-nm unit as indicated by red arrows. PF pair-A8/A9 is shown as an example. (C) Plot of inter-PF angles from sonicated A-tubule map. Values of the doublet and sarkosyl A-tubule from Fig. 5F are shown in gray for comparison. Two-way ANOVA followed by Tukey's multiple comparison test was performed for statistical analysis. Curvatures of PFs A5-A9, where MIPs are preserved are the least affected. (D and E) Comparison of PF pair-A12/A13 models from doublet and sarkosyl A-tubule. View in (D) is the same as Fig. 5G. The models are aligned by the tubulin dimer in PF-A12. The display model is from the PF pair-A12/A13 of the doublet and colored based on the displacement of Cα. The displacement vectors from the doublet to the sarkosyl A-tubule are shown in red. The displacement vectors clearly show the rotation of the tubulin dimer in A13 in the sarkosyl A-tubule. Yellow, nucleotides.

Table S1. Tubulin dimer distances of the A-tubule lattice.

	Dimer distances (intra- / inter-dimer distances) from doublet (Å) (mean ± SD, n = 6)	Dimer distances (intra- / inter-dimer distances) from sonicated A-tubule (Å) (mean ± SD, n = 6)	Dimer distances (intra- / inter-dimer distances) from sarkosyl A-tubule (Å) (mean ± SD, n = 6)
A1	83.1 ± 0.309 (41.8 ± 0.0352 / 41.3 ± 0.299)	83.1 ± 0.313 (41.8 ± 0.222 / 41.3 ± 0.300)	81.0 ± 0.333 (41.1 ± 0.106 / 39.9 ± 0.253)
A2	83.3 ± 0.0354 (41.7 ± 0.0507 / 41.5 ± 0.0636)	83.3 ± 0.0672 (41.8 ± 0.0474 / 41.6 ± 0.0796)	81.2 ± 0.143 (41.0 ± 0.0868 / 40.2 ± 0.0929)
A3	83.4 ± 0.0988 (41.8 ± 0.0242 / 41.6 ± 0.0975)	83.5 ± 0.0696 (41.8 ± 0.0351 / 41.7 ± 0.0549)	81.4 ± 0.0965 (40.8 ± 0.0455 / 40.6 ± 0.0965)
A4	83.5 ± 0.274 (41.8 ± 0.0460 / 41.6 ± 0.255)	83.6 ± 0.195 (41.8 ± 0.0457 / 41.8 ± 0.191)	81.5 ± 0.242 (40.8 ± 0.0511 / 40.7 ± 0.215)
A5	83.4 ± 0.184 (41.9 ± 0.0414 / 41.6 ± 0.199)	83.6 ± 0.127 (41.9 ± 0.0344 / 41.8 ± 0.154)	81.4 ± 0.0944 (40.7 ± 0.118 / 40.7 ± 0.198)
A6	83.3 ± 0.369 (41.8 ± 0.0730 / 41.5 ± 0.345)	83.5 ± 0.271 (41.8 ± 0.0586 / 41.7 ± 0.224)	81.4 ± 0.206 (41.0 ± 0.112 / 40.4 ± 0.216)
A7	83.1 ± 0.228 (41.7 ± 0.0762 / 41.4 ± 0.192)	83.3 ± 0.0896 (41.8 ± 0.558 / 41.5 ± 0.102)	81.3 ± 0.175 (41.0 ± 0.0914 / 40.3 ± 0.109)
A8	82.9 ± 0.319 (41.7 ± 0.0786 / 41.2 ± 0.253)	83.0 ± 0.182 (41.7 ± 0.0337 / 41.3 ± 0.173)	81.1 ± 0.204 (40.8 ± 0.0403 / 40.2 ± 0.207)
A9	82.8 ± 0.367 (41.7 ± 0.0653 / 41.0 ± 0.337)	82.8 ± 0.198 (41.7 ± 0.0650 / 41.1 ± 0.239)	80.9 ± 0.285 (40.9 ± 0.138 / 40.1 ± 0.295)
A10	82.7 ± 0.221 (41.6 ± 0.0545 / 41.0 ± 0.218)	82.7 ± 0.202 (41.7 ± 0.0753 / 41.0 ± 0.226)	80.8 ± 0.268 (40.7 ± 0.104 / 40.1 ± 0.261)
A11	82.7 ± 0.676 (41.7 ± 0.0840 / 41.0 ± 0.649)	82.6 ± 0.575 (41.7 ± 0.0583 / 41.0 ± 0.593)	80.7 ± 0.610 (40.7 ± 0.0681 / 40.0 ± 0.590)
A12	82.7 ± 0.875 (41.6 ± 0.0900 / 41.1 ± 0.960)	82.7 ± 0.912 (41.7 ± 0.0462 / 41.0 ± 0.938)	80.8 ± 0.836 (40.7 ± 0.0542 / 40.1 ± 0.865)
A13	82.9 ± 0.870 (41.7 ± 0.0443 / 41.2 ± 0.908)	82.9 ± 0.820 (41.7 ± 0.0304 / 41.1 ± 0.836)	80.9 ± 0.772 (40.7 ± 0.0775 / 40.1 ± 0.833)
All*	83.1 ± 0.540 (41.7 ± 0.0937 / 41.3 ± 0.516)	83.1 ± 0.546 (41.8 ± 0.0810 / 41.4 ± 0.516)	81.1 ± 0.485 (40.8 ± 0.158 / 40.3 ± 0.483)

*For all PF results, mean values with SD calculated from all PFs (n = 78) are shown

Table S2. Summary of Bonferroni's multiple comparisons test of tubulin dimer distances comparing doublet and sarkosyl A-tubule.

	Mean differences (Å)	95% confidence intervals of differences	Adjusted *p*-values
A1	2.056	1.255 to 2.857	< 0.00010
A2	2.043	1.243 to 2.844	< 0.00010
A3	2.036	1.235 to 2.837	< 0.00010
A4	1.977	1.176 to 2.778	< 0.00010
A5	1.992	1.191 to 2.793	< 0.00010
A6	1.901	1.100 to 2.702	< 0.00010
A7	1.861	1.060 to 2.662	< 0.00010
A8	1.853	1.052 to 2.653	< 0.00010
A9	1.834	1.033 to 2.635	< 0.00010
A10	1.87	1.069 to 2.671	< 0.00010
A11	1.915	1.114 to 2.716	< 0.00010
A12	1.95	1.149 to 2.751	< 0.00010
A13	2.005	1.204 to 2.806	< 0.00010

Table S3. Angles between PFs.

	Doublet (°) (mean ± SD, n = 4)	Sonicated A-tubule (°) (mean ± SD, n = 4)	sarkosyl A-tubule (°) (mean ± SD, n = 4)
A1/A2	26.1 ± 0.341	24.9 ± 0.231	24.2 ± 0.448
A2/A3	33.7 ± 0.303	33.3 ± 0.0913	32.9 ± 0.159
A3/A4	28.7 ± 0.273	29.4 ± 0.295	29.6 ± 0.410
A4/A5	27.1 ± 0.426	27.2 ± 0.125	27.8 ± 0.458
A5/A6	23.6 ± 0.571	23.2 ± 0.211	23.8 ± 0.505
A6/A7	22.2 ± 0.542	22.3 ± 0.245	22.2 ± 0.358
A7/A8	32.0 ± 0.596	32.6 ± 0.261	32.2 ± 0.304
A8/A9	22.9 ± 0.229	22.6 ± 0.115	22.5 ± 0.254
A9/A10	41.1 ± 0.122	40.3 ± 0.351	40.0 ± 0.243
A10/A11	29.2 ± 0.367	29.1 ± 0.336	28.3 ± 0.523
A11/A12	20.8 ± 0.577	20.5 ± 0.291	21.7 ± 0.393
A12/A13	16.9 ± 0.480	17.9 ± 0.241	19.6 ± 0.115
A13/A1	35.8 ± 0.542	36.5 ± 0.286	35.4 ± 0.414

Table S4. Summary of Bonferroni's multiple comparisons test of PF-pair angles comparing doublet and sarkosyl A-tubule.

	Mean differences (°)	95% confidence intervals of differences	Adjusted *p*-values
A1/A2	1.96	0.9693 to 2.951	< 0.00010
A2/A3	0.7659	-0.2249 to 1.757	0.3111
A3/A4	-0.9081	-1.899 to 0.08273	0.1015
A4/A5	-0.7241	-1.715 to 0.2667	0.422
A5/A6	-0.2226	-1.214 to 0.7682	> 0.9999
A6/A7	-0.06678	-1.058 to 0.9241	> 0.9999
A7/A8	-0.2326	-1.223 to 0.7582	> 0.9999
A8/A9	0.3308	-0.6600 to 1.322	> 0.9999
A9/A10	1.172	0.1816 to 2.163	0.0092
A10/A11	0.9591	-0.03173 to 1.950	0.0659
A11/A12	-0.8835	-1.874 to 0.1073	0.1243
A12/A13	-2.658	-3.649 to -1.667	< 0.00010
A13/A1	0.38	-0.6109 to 1.371	> 0.9999

Table S5. Tubulin dimer distances of the B-tubule from doublet.

	Dimer distances from doublet B-tubule (Å) (mean ± SD, n = 6)
B1	82.4 ± 0.258
B2	82.3 ± 0.476
B3	82.2 ± 0.422
B4	82.2 ± 0.395
B5	82.2 ± 0.401
B6	82.2 ± 0.502
B7	82.4 ± 0.111
B8	82.5 ± 0.581
B9	82.8 ± 0.443
B10	82.9 ± 0.195
All*	82.4 ± 0.468

*For all PF results, mean values with SD calculated from all PFs (n = 60) are shown

Supplementary movie legends

Movie S1. Complex network of MIPs inside the doublet tubulin lattice.
MIPs inside the doublet tubulin lattice are connected and form a complex network. Some branches even reach the outside surface.

Movie S2. Rib43a are the fMIPs in the PF ribbon region.

Movie S3. Coarse grain molecular dynamic simulation of a three-dimer protofilament with Rib43a-S.

Movie S4. Coarse grain molecular dynamic simulation of a three-dimer protofilament without Rib43a-S.

Movie S5. Comparison of tubulin lattice models from doublet and sarkosyl A-tubule.
Tubulin models based on PF-A12 are morphed. After the sarkosyl treatment, tubulin lattice shows a significant longitudinal compaction.

Supplementary References and Notes

1. S. El-Gebali *et al.*, The Pfam protein families database in 2019. *Nucleic Acids Res* **47**, D427-D432 (2019).